Solar Physics (2006) 234: 21–40
DOI: 10.1007/s11207-006-2091-0

THE MAGNETIC FIELD, HORIZONTAL MOTION AND HELICITY IN A FAST EMERGING FLUX REGION WHICH EVENTUALLY FORMS A DELTA SPOT

JIHONG LIU and HONGQI ZHANG
National Astronomical Observatories, Chinese Academy of Sciences, 100012 Beijing, China
(e-mail: ljh@sun10.bao.ac.cn)

(Received 7 May 2005; accepted 6 December 2005)

Abstract. We studied the behavior of magnetic field, horizontal motion and helicity in a fast emerging flux region NOAA 10488 which eventually forms a δ spot. It is found that the rotation of photospheric footpoints forms in the earlier stage of magnetic flux emergence and the relative shear motion of different magnetic flux systems appears later in this active region (AR). Therefore the emerging process of the AR can be separated into two phases: rotation and shear. We have computed the magnetic helicity injected into the corona using the local correlation tracking (LCT) technique. Furthermore we determined the vertical component of current helicity density and the vertical component of induction electric fields $E_z = (\mathbf{V} \times \mathbf{B})_z$ in the photosphere. Particularly we have presented the comparison of the injection rate of magnetic helicity and the variation of the current helicity density. The main results are as follows: (1) The strong shear motion (SSM) between the new emerging flux system and the old one brings more magnetic helicity into the corona than the twisting motions. (2) After the maturity of the main bipolar spots, their twist decreases and the SSM becomes dominant and the major contributor of magnetic non-potentiality in the solar atmosphere in this AR. (3) The positions of the maxima of E_z (about $0.1 \sim 0.2\,\mathrm{V\,cm^{-1}}$) shift from the twisting areas to the areas showing SSMs as the AR evolved from the rotation phase to the shear one, but no obvious correlation is found between the kernels of Hα flare and E_z for the M1.6 flare in this AR. (4) The coronal helicity inferred from the horizontal motion of this AR amounts to $-6 \times 10^{43}\,\mathrm{Mx^2}$. It is comparable with the coronal helicity of ARs producing flares with coronal mass ejections (CMEs) or helicity carried away by magnetic clouds (MCs) reported in previous studies (Nindos, Zhang, and Zhang, 2003; Nindos and Andrews, 2004). In addition, the formation of the δ configuration in this AR belongs to the third formation type indicated by Zirin and Liggett (1987), i.e., collision of opposite polarities from different dipoles, and can be naturally explained by the SSM.

1. Introduction

It is generally believed that the magnetic field is generated near the bottom of the convective zone and emerges to the solar surface where it forms solar active regions. Both magnetic energy and helicity are brought into the corona with the magnetic flux as the field emerges. The magnetic energy released in solar active phenomena, such as flares and CMEs, is provided by the non-potential components of the magnetic field in ARs. There are some possibilities for the accumulation of non-potential magnetic energy in the solar atmosphere. One is that the twisted magnetic flux emerges to form the observed twisted magnetic ropes or magnetic

knots in delta ARs (Tanaka, 1991; Wang, Xu, and Zhang, 1994; Leka *et al*., 1996; Liu and Zhang, 2001). Another possibility is magnetic shear or squeeze between different magnetic structures of ARs in the photosphere which reflect the interaction of different magnetic flux systems with free magnetic energy accumulating in the solar corona (Hagyard *et al*., 1984; Chen, Wang, and Zirin, 1994; Zhang, 2001a,b; Deng *et al*., 2001). The interaction of different magnetic flux systems actually arises from the emergence of new magnetic flux.

Magnetic helicity has close relation with the generation of the magnetic field and the solar activity on the solar surface. It is conserved in a closed volume under the ideal MHD condition. But in an open volume such as the solar atmosphere, it is not conserved. It may be transported from sub-photosphere to the solar corona through the solar surface either via the passage of helical magnetic field lines from below or via the shuffling of footpoints of pre-existing coronal field lines (Berger and Field, 1984). The latter term has been observationally determined by Chae (2001) from a time series of line-of-sight magnetograms with the LCT method suggested by November and Simon (1988). It has been realized by Démoulin and Berger (2003) that the helicity computed with the LCT method yields not only the helicity injected from shearing motions but also the helicity coming from flux emergence. In recent years, the photospheric flux of magnetic helicity has been computed by many researchers in the study of flares, filaments, CMEs and MCs (Chae *et al*., 2001; Moon *et al*., 2002a,b; Nindos and Zhang, 2002; Kusano *et al*., 2002; Nindos, Zhang, and Zhang, 2003; Nindos and Andrews, 2004; Yang *et al*., 2004).

Current helicity is an important diagnostic of non-potentiality in solar atmosphere. For the observing limitation, only the vertical component of the current helicity density, i.e.

$$hc_{\parallel} = B_{\parallel} \cdot (\nabla \times \mathbf{B})_{\parallel}, \tag{1}$$

can be deduced from the available vector magneograms (Bao and Zhang, 1998). From the evolution of the current helicity density we can get some information on the generation of the twisted magnetic field below the photosphere. The hemispheric sign rule of the current helicity in the solar active regions was discovered by Seehafer (1990): In a statistical sense, on the Northern/Southern hemisphere ARs carry negative/positive helicity. The current helicity density has close relationship with solar activity events. The relationship between the flare occurrence in the solar ARs with the reversed helicity sign for their hemisphere was presented by Bao, Ai, and Zhang (2001). The theoretical interpretation of the flare activity and changes in electric current helicity was presented by Kim *et al*. (2002). The relationship between helicity evolution and δ-configurations was studied by Liu and Zhang (2002). The helicity patterns of CME-associated ARs were analyzed by Wang, Zhou, and Zhang (2004).

Physically speaking, the induction electric field, $\mathbf{E} = \mathbf{V} \times \mathbf{B}$, corresponds to the motion of magnetic field lines on the solar surface and probably has some

relationship with the non-potentiality in solar atmosphere. In this paper, we discuss just the vertical component of **E**, that is,

$$E_z = (\mathbf{V} \times \mathbf{B})_z, \tag{2}$$

which shows the relationship between the horizontal motion and the transverse magnetic field. We deduce E_z in the photosphere from transverse magnetic fields derived from vector magnetograms and horizontal velocities computed by LCT technique. Such work has not been reported before.

The formation of δ configuration is an important problem in the study of the photospheric magnetic field. Zirin and Liggett (1987) classified the formation of δ spots in three types: emergence of a single complex AR formed below the surface, emergence of large satellite spots near a large older spot, or collision of spots of opposite polarity from different dipoles. Liu and Zhang (2002) reported an exceptional formation pattern of δ configuration, i.e., rapid coalescence of two opposite magnetic features in a pre-existing δ configuration. Obviously the formation of the δ configuration in AR 10488 belongs to the third formation type indicated by Zirin and Liggett (1987). Tang (1983) examined δ formation of such type. With the convenience of the combined data set of line-of-sight magnetograms taken by the Michelson Doppler Imager (MDI) and vector magnetograms taken at Huairou Solar Observing Station (HSOS), we have the opportunity to examine the formation and the behavior of this δ spot.

In this paper, we focus on the transport and accumulation of the magnetic helicity and non-potentiality of AR NOAA 10488. This AR is a fast emerging flux region. One magnetic flux system emerged from the sub-photosphere firstly showing significant footpoint rotation. Two new magnetic flux systems emerged later exhibiting strong shear motions relative to the old flux system. The former no longer show obvious rotation of the footpoints any longer after the emergence of the new magnetic fluxes. Eventually a δ spot forms. Such evolution process shows the twist and interaction of magnetic flux systems in two successive steps, while forming a single AR. Thus it is possible for us to compare the roles played by the twist of a single magnetic flux system and the interaction of different magnetic flux systems in the transport and accumulation of magnetic helicity and non-potentiality, which are still not well understood. Since both magnetic helicity and current helicity density have been analyzed, their relations can be explored. The E_z in the photosphere has been studied particularly, which has been very rarely inferred from the observational data before. Our data and the analysis method are introduced in Section 2. Investigations of magnetic field, horizontal motion, transport of magnetic helicity, current helicity density and E_z are presented in Section 3. Some discussions are presented in Section 4. A brief summary is given in Section 5.

2. Data and Method

We use a set of MDI 1 min full-disk longitudinal magnetograms, which were obtained from 13:00 UT on 2003 October 26 to 22:00 UT on October 31. The full-disk magnetograms are recorded by a 1024 × 1024 CCD detector with a pixel size of 2″. The field of view of the magnetograms that we analyze is 400″ × 400″, covering the whole of AR NOAA 10488. The reference time has been chosen to be 18:00 UT on 2003 October 28, when the AR passed through the central meridian.

MDI magnetogram data suffer from instrumental effects. It is found that MDI underestimated the flux densities in a linear way for MDI pixels below 1200 G by approximately a factor of 1.54 (Berger and Lites, 2003). A nonlinear correction formula was presented to give the corrected MDI flux below and above 1200 G separately (Nindos, Zhang, and Zhang, 2003). But we carry out the LCT using the original MDI data, which gives the lower limit of the computation.

The transport rate of magnetic helicity from the sub-photosphere to corona by the photospheric horizontal motions is described by the equation

$$\frac{\mathrm{d}H}{\mathrm{d}t} = -2 \oint (\mathbf{A}_p \cdot \mathbf{u}) B_n \mathrm{d}^2 x, \tag{3}$$

where $\mathbf{A}_p$ is the vector potential of the potential field, $\mathbf{u}$ is the velocity computed by the tracking method, B_n is the normal component of magnetic field. We have computed the transport rate of helicity with the LCT technique following Chae *et al*. (2001). The nonlinear mapping, flux density interpolation and the geometrical foreshortening correction all have been done following the method by Chae *et al*. (2001). Thus, the LCT is applied to magnetograms from which the effect of solar differential rotation had been removed; the resulting magnetograms have new grids with pixel size of 1″; and the vertical field strength becomes equal to the line-of-sight field strength times $1/\cos\psi$, where ψ is the heliocentric angle of the region. To increase the signal-to-noise ratio we take time average by integrating five successive magnetograms with 1 min cadence. We follow Chae *et al*. (2001) to choose the FWHM of the apodizing function as 8″ and the time interval as 20 min, and to set the horizontal velocity in regions with low flux density (<10 G) or low cross-correlation value (<0.9) to zero to reduce the noise effects. To minimize the effect of the periodic boundary condition, the domain for A_p computation is set to have 9 times as large an area as the analyzed field of view.

Fine photospheric vector magnetograms were obtained on October 27–30 by HSOS magnetograph from which we calculate the vertical component of current helicity density. The 180° ambiguity for the transverse field components is resolved with a linear force-free field method to best fit the azimuth (Wang and Abramenko, 2000). The transformation of the magnetic field vector and the geometric mapping of the observed field in the image plane into the heliographic plane is done following Gary and Hagyard (1990).

3. Magnetic Field, Horizontal Motion and Helicity

3.1. Evolution of magnetic field

The evolution of longitudinal magnetic field of AR 10488 is presented in Figure 1. This AR passed across the solar disk from October 26 to November 3 (Zhang *et al.*, 2003) and was located in the latitudinal zone $7^\circ < b < 9^\circ$ during the period of our observation. The main bipolar spots emerged very fast from the east of the central meridian at 11:00 UT on 2003 October 26, simultaneously rotating clockwise rapidly. At about 17:00 UT on October 27, a pair of new bipolar spots began emerging to the east of the main spots. They grew fast and approached the main bipolar spots gradually. Another set of small bipolar spots emerged to the north of the main bipolar spots from October 28. Since they did not show significant shearing motions with the old bipolar spots during the observing period, we do not discuss them further in this paper. By October 29, the AR became a δ-configuration. Taken the constancy of the separation between two opposite polarities as the criterion of AR's maturity, the main bipolar sunspots became mature by October 29. At that time the AR did not show obvious rotation motion any longer and obeyed Hale's Law. After 8:00 UT on October 29, the positive spot of the new emerging bipole east to the main spots kept shearing strongly with the negative spot of the main bipole. So the magnetic evolution of the AR can be separated into two stages. We define the stage before 8:00 UT on October 29, when the rotation of photospheric footpoints was present as the *rotation phase* and the one after that time when the strong shear motion (SSM) of two different magnetic flux systems was present as the *shear phase*.

In the first column of Figure 2 we show the vector magnetograms after projection-effect correction. As the AR was not far from the central meridian between October 27–30, the correction of the projection effect of the vector magnetic field is quite small. The negative spot marked 'c' always had left-handed twist. The leading positive spot had right-handed twist on October 27 and 28. The upper part of the leading positive spot where marked 'a' held right-handed twist on October 29 and 30, while the lower part marked 'b' had weak left-handed twist at that time. Further discussion about the twist of the AR will be presented later.

The computed horizontal velocity vectors are shown in the second column of Figure 2. The spiral directions of the velocity vectors in most of the area of the AR are opposite to those of the transverse magnetic fields. For example, on October 27, the velocity vectors direct to clockwise, opposite to the rotation direction of the transverse field. On October 28, the velocity vectors both in the lower part of the leading positive spot marked 'B' and in most areas of the negative following spot marked 'C' direct oppositely to the transverse fields. The conditions on October 29 and 30 are similar to that of 28. On October 29 and 30, the velocity vectors in the upper part of the leading positive spot marked 'A' have opposite rotation to that of

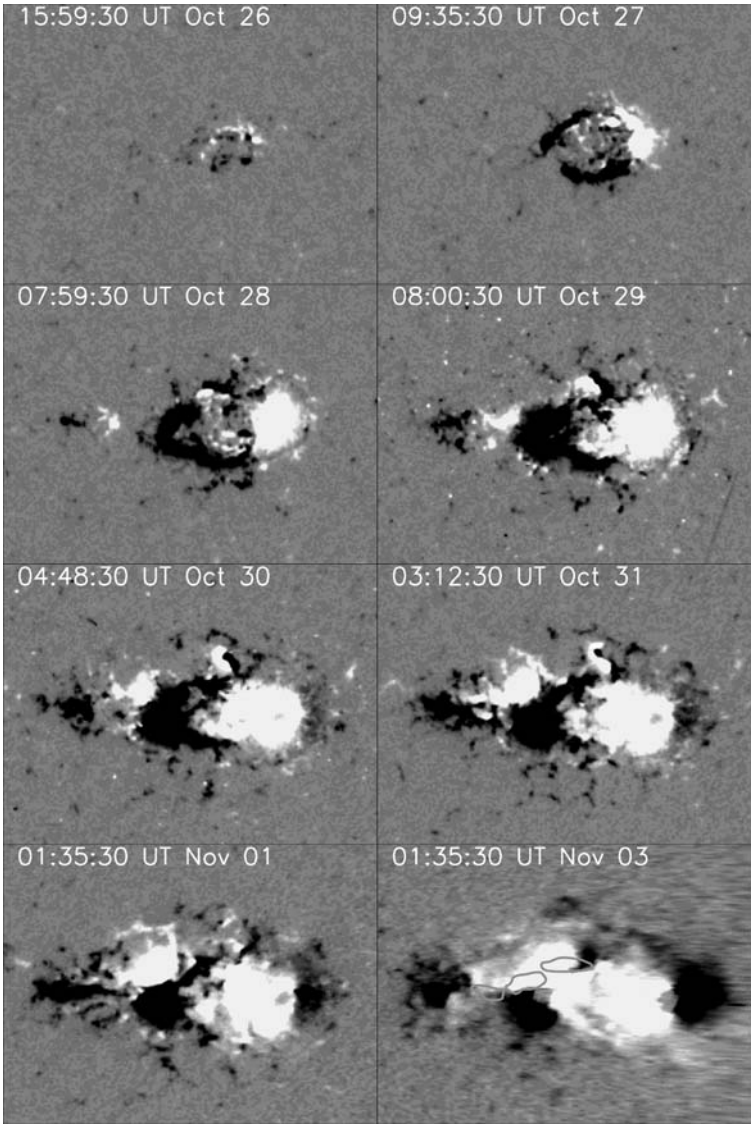

Figure 1. MDI longitudinal magnetograms of AR 10488 between 2003 October 26 and November 3. The superposed *contours* in the last map represent the flare kernels in the Hα image of HSOS at 01:25 UT on November 3, which have undergone geometrical foreshorten correcting. The field of view is $400'' \times 300''$.

the transverse field, too. However, they have a spiral pattern similar to that of the transverse field on October 28.

The transverse magnetic fields can be regarded as the horizontal projections of the spiral magnetic fluxes. The transverse velocities computed by the LCT method

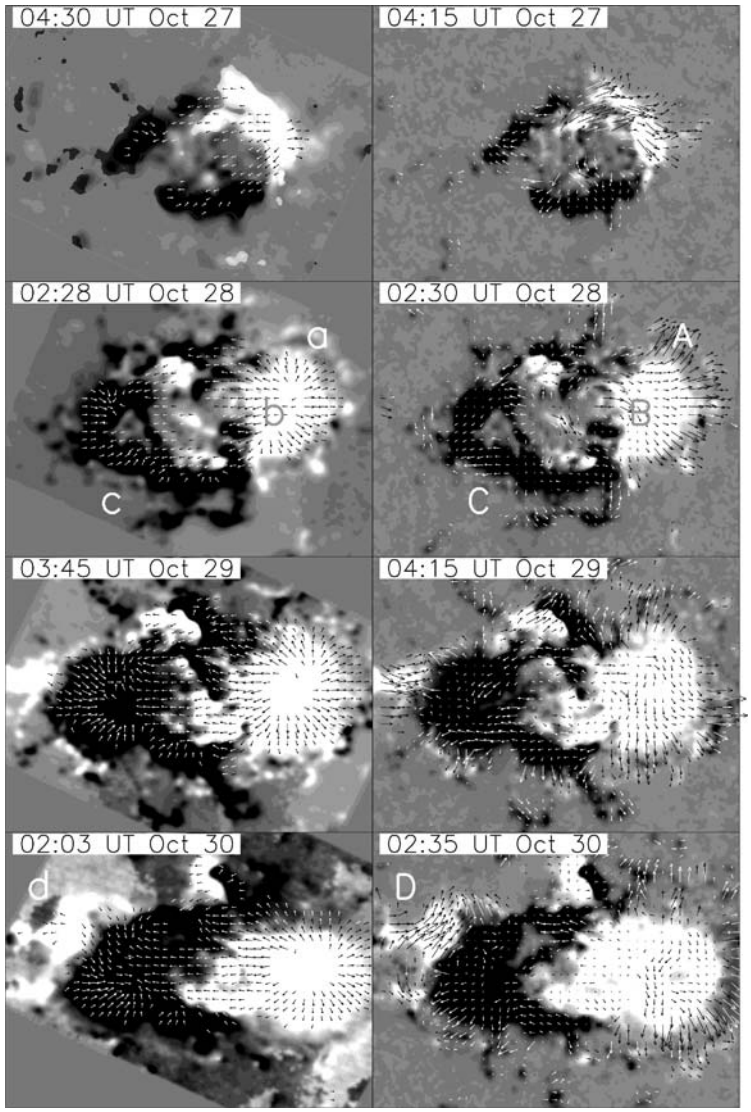

Figure 2. Vector magnetograms of HSOS (*left*) and computed horizontal velocity vectors being superposed on MDI longitudinal magnetograms (*right*). The maximum *arrow* length measures transverse magnetic field of 1200 G and velocity of 0.8 km s^{-1}, respectively. The field of view is $225'' \times 168''$.

represent the horizontal motions of the footpoints of the magnetic field lines. So when a magnetic flux tube emerges from the sub-photosphere, the footpoints of the magnetic field should rotate in opposite direction to the spirals of the transverse magnetic field lines. This is confirmed by the observational result shown in Figure 2. As for the contrary case of 'A' area on October 28, it is probably due to the fast expansion of the magnetic flux during its fast emergence.

Let's pay attention to the area marked 'D'/'d' in Figure 2. Since October 29, the SSM between the positive part of the new emerging bipolar spots and the old negative spot becomes stronger and stronger. In this area, the transverse magnetic fields have weak left-handed twist and the velocity vectors have strong right-handed rotation. It may imply the emergence of a new magnetic flux system with left-handed twist from below to the photosphere. However, the SSM is more obvious than the twist there and is probably more important.

3.2. TRANSPORT OF MAGNETIC HELICITY

Figure 3b and c display the temporal variation of the rate of helicity changes, $\mathrm{d}H/\mathrm{d}t$, deduced from horizontal motions, and of the accumulated change of helicity, $\Delta H(t)$, calculated from the measured $\mathrm{d}H/\mathrm{d}t$, separately. There are time intervals when no $\mathrm{d}H/\mathrm{d}t$ measurements are available owing to the lack of high-cadence MDI data. Following Nindos and Zhang (2002), we estimate these missing $\mathrm{d}H/\mathrm{d}t$ values by spline interpolation. The resulting ΔH curve is presented in Figure 3c with thin line. The temporal variations of $\mathrm{d}H/\mathrm{d}t$ and ΔH show that during the AR's development the rate of helicity change is negative, and the absolute value of the accumulated change of magnetic helicity is increasing. October 29 is a critical time for the magnetic helicity change. Before about 8:00 UT on October 29, that is, in the rotation phase, the $\mathrm{d}H/\mathrm{d}t$ is small and the helicity change is rather slow. In the shear phase, the $\mathrm{d}H/\mathrm{d}t$ is rather large and the helicity change becomes fast and significant. In approximately equal time duration, the accumulated change of the magnetic helicity in the shear phase is about 3 times larger than that of the rotation phase. That the SSM brings more magnetic helicity into the corona than the twist implies that the interaction of two different flux systems brings more helicity into the upper atmosphere than the twist of a single flux system in this AR.

However, should we consider that the SSM between different flux systems is more effective in helicity transport than the twist of a single flux system? Or should we attribute the low rate of transport of helicity before October 29 to the low magnetic flux? To check the dependence of the helicity on the flux, we calculated the accumulated change of helicity divided by the square of the magnetic flux. Figure 3a displays the positive and negative fluxes of the AR as function of time. Supposing the magnetic field of the AR was twisted as a whole, the ratio H/F^2, as is shown in Figure 4, corresponds to the number of end-to-end turns in the AR. As the AR is emerging from the sub-photosphere, the twist is generally brought into the upper atmosphere, manifested by an increase of the absolute value of H/F^2. From Figure 4 we find that 5.5 days after the AR's birth, the H/F^2 reaches -0.04. This value is in agreement with the ones reported by previous works (Chae, Moon, and Park, 2004 and references there in). We also find that the increasing rate of H/F^2

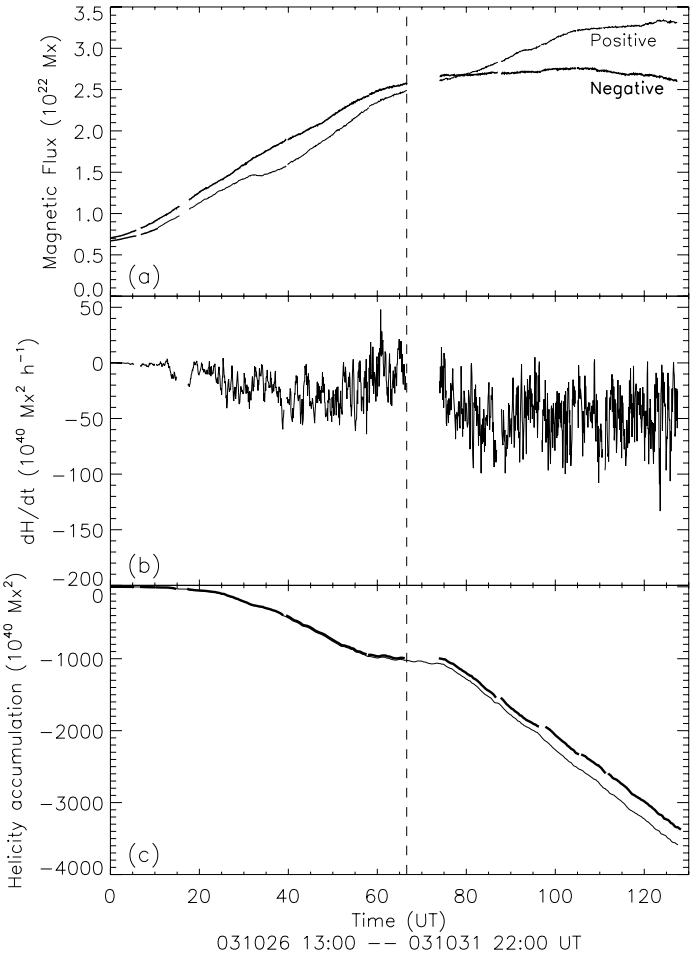

Figure 3. (a) Time profile of the AR's longitudinal magnetic field flux derived from full-disk MDI images. (b) Time profile of the rate of helicity injected by horizontal motions. (c) Time profile of the accumulated change of helicity $\Delta H(t)$ calculated from the measured $\mathrm{d}H/\mathrm{d}t$ (*thick line*) and the estimated $\Delta H(t)$ if a spline interpolation is used for the determination of the missing $\mathrm{d}H/\mathrm{d}t$ values (*thin line*). The *dashed line* indicates the time separating the rotation and shear phases.

in the shear phase is very close to that of the former 50 h of the rotation phase. So for AR 10488, both the twist and the SSM are effective in helicity transport.

However, we also find from Figure 4 that the absolute value of H/F^2 does not increase any more and even decreases a little in the last 16 h of the rotation phase, which implies a decrease of the overall magnetic helicity of the AR in that stage. In the subsequent shear phase, the absolute value of H/F^2 increases significantly and persistently, which is due to the SSM between the new emerging flux system and the old one. So the SSM between two different magnetic flux systems in this AR is indeed the major contributor to the helicity injection.

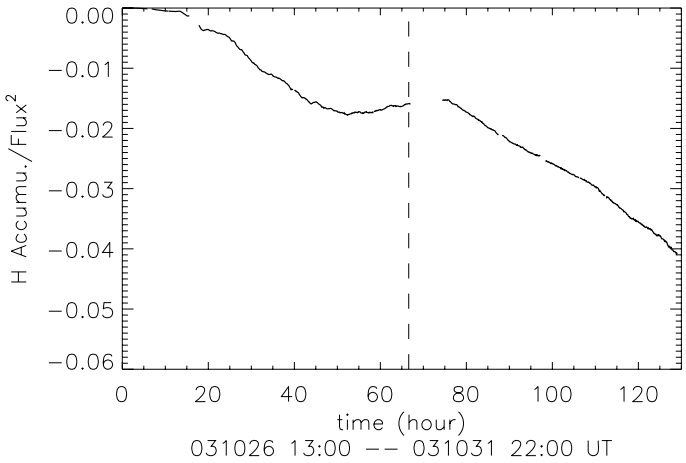

Figure 4. Ratio of the coronal helicity accumulation to the square of the magnetic flux. The *dashed line* indicates the time separating the rotation and shear phases.

An easy way to evaluate the physical significance of the observed flow on the transport of magnetic helicity is to examine the distribution of $G \equiv -2(\mathbf{u} \cdot \mathbf{A}_p)B_z$. It is a measure of the local contribution of the foot-point motion to the rate of the transport of magnetic helicity (Chae, 2001). Figure 5 shows the gray scale map of G at specific times. Since we are interested in the large-scale trends of the helicity variability, the maps of G are 1 h averages around the times indicated in each map. In the rotation phase, the maxima of G are located mainly in the rotating or twisting area of the main positive spot. In the shear phase, the maxima of G are located mainly near the magnetic neutral line between the new emerging positive spot and the old negative spot where intense shearing motions took place (marked by the white rectangle). This further confirms our above conclusion.

3.3. Current helicity density

The vertical component of current helicity density provides some information on the local twisting of magnetic field in the photosphere. (We call the vertical component of current helicity density *current helicity density* for writing convenience hereafter). The gray-scale maps of the current helicity density, $hc_\parallel$, for the areas of $B_\parallel > 200G$ are shown in the first column of Figure 6. The maps of $hc_\parallel$ are one or few hours averages around the times indicated in each map. The mean current helicity density in the figure at 04:30 on October 27, 02:28 on October 28, 03:45 on October 29, 02:03 on October 30 are -1.8, -4.0, -4.8, -4.6 respectively (the unit is $10^{-3}\,\mathrm{G}^2\,\mathrm{m}^{-1}$). The sign of the mean current helicity density of the AR is negative, same as that of the ΔH. That the accumulated change of magnetic helicity is of the same sign as the chirality of the AR means that the computed photospheric

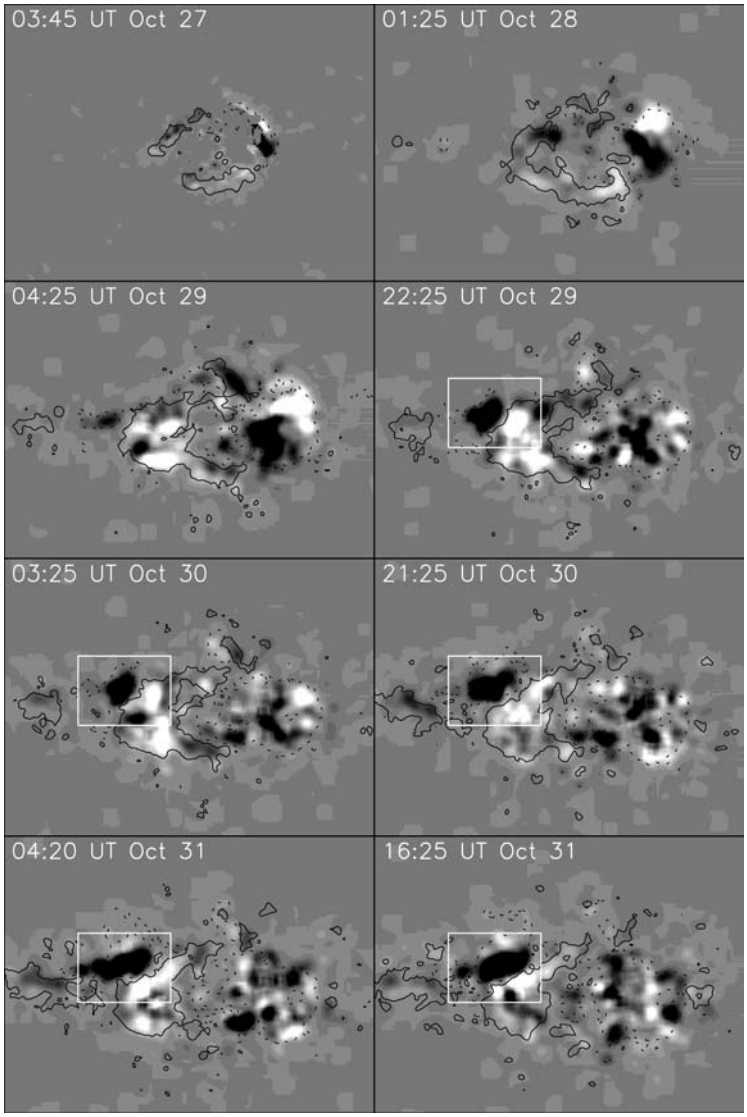

Figure 5. Gray-scale maps of $G \equiv -2(\mathbf{u} \cdot \mathbf{A}_p)B_z$ of 1 h averages. The *white* and *black colors* indicate the positive and negative signs of G, respectively. The *white rectangles* mark the areas of maxima of G which correlate with SSM. The *dashed* and *full contours* represent longitudinal magnetic field strengths of ± 200 G, the field of view is $400'' \times 300''$.

motions contribute to the increase of the amount of the coronal magnetic helicity. The amount of the mean current helicity density of the AR approximately increase with time. However, from October 29 to October 30, it shows no obvious increase, but on the contrary, a small decrease. The field of view of magnetograms obtained at HSOS is not large enough for this AR and covers only the main spots and a

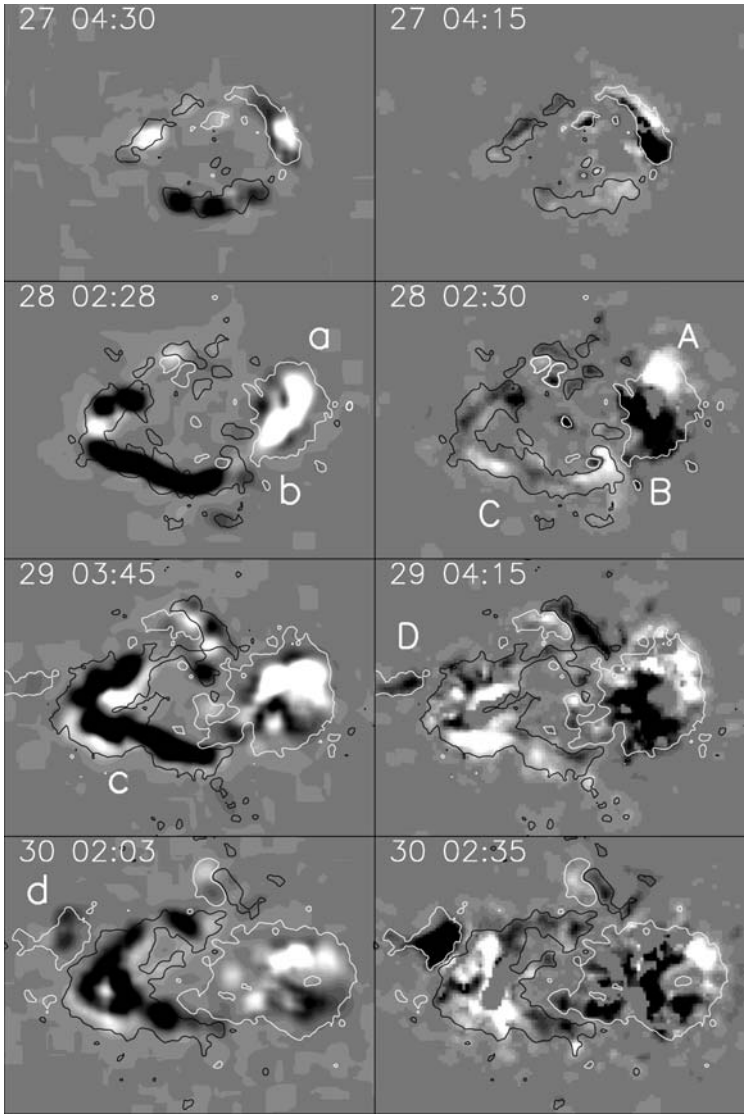

Figure 6. Gray-scale maps of the time averages of current helicity density $hc_{\parallel}$ (*left*) and the time averages of $-2(\mathbf{u}\cdot\mathbf{A}_p)B_z$ (*right*). The *white* and *black contours* represent longitudinal magnetic field strengths of 200 and -200 G, respectively. The field of view is $225'' \times 168''$.

small part of the new emerging spots. Thus the deduced current helicity density is dominantly of the main spots. We find that after the maturity of the main bipolar spots, their twist remains steady or decreases.

To compare the current helicity density with the transport of magnetic helicity, we show the gray-scale maps of G at the corresponding times in the second column

of Figure 6. The maps of G are also one or few hours averages around the times indicated in each map. Although the two parameters have the same negative sign in sum for each map, they have opposite signs in most of the local distributions. The G factor is a measure of the local contribution of the foot-point motion to the rate of the transport of magnetic helicity. So the area with positive sign of G will have higher magnetic helicity at the subsequent time than that of the current moment, that is, increased positive helicity or decreased negative helicity. The magnetic helicity and current helicity are all descriptions of the spiral character of the magnetic field. Therefore their evolution should be correlated some way. So in an area, where G and $hc_{\|}$ have opposite signs, the intensity of $hc_{\|}$ will probably decrease later on. However, the injection rate of magnetic helicity and photospheric density of current helicity reflect different aspects of magnetic helicity. Therefore the injected magnetic helicity is probably not proportional to the current helicity density in the photosphere.

This can be confirmed by the helicity evolution of AR 10488, as is shown in Figure 6. From October 28, the intensity of the local current helicity density increases on the following day in most areas where the G and $hc_{\|}$ have the same sign, and decrease in most areas where the G and $hc_{\|}$ have opposite signs. For example, on October 28, a part of the preceding component of the main sunspots has positive G and positive $hc_{\|}$ (marked 'A' and 'a' in the maps of the two parameters separately in Figure 6), and the current helicity density in this area increases in absolute value on October 29. For the area marked 'B' and 'b' separately which has opposite sign of G and $hc_{\|}$, the current helicity density decreases from being positive on October 28 to a weak negative value on October 29. Most parts of both preceding and following components of the main sunspots have opposite signs of G and $hc_{\|}$ on October 29, therefore the intensity of current helicity density on October 29 decreases obviously to the weaker distribution on October 30. Most parts of the main spots continue to have opposite signs of G and $hc_{\|}$ on October 30, so we can predict that the intensity of the current helicity density there will probably decrease on the next day. So it is well possible that the twist of the main bipolar spots decreases after they reach maturity on October 29.

However, the current helicity density on October 28 obviously does not follow the evolution of G and $hc_{\|}$ on October 27, which may be related to the fast flux emergence. And for the area marked 'C' and 'c' which has positive G and negative $hc_{\|}$ on October 28, there is no obvious intensity decrease of $hc_{\|}$ on October 29. These show the unproportionate cases of the magnetic helicity injected into corona and the current helicity density in the photosphere.

It is worth paying attention to the areas marked 'D' and 'd' in the maps of the two parameters in Figure 6. It is a positive magnetic feature and shears strongly with the old negative following spot. The area has negative G and no obvious current helicity density on October 29. On October 30, negative current helicity density appears in this area. The G there remains negative on October 30, so we can predict that the intensity of the current helicity density there will increase on

the next day. Unfortunately we do not have vector magnetograms to investigate the non-potentiality in the shear phase. However, at 01:25 UT on November 3 three flare (X-class) kernels being located right between the new positive spot and the old negative spot were observed by the HSOS Hα telescope (See the contours on the last map in Figure 1). No X-class flares occurred before in this AR. Although the exact change of magnetic configuration right before the flare is not known, there is no doubt that the SSM contributes significantly to the transport and accumulation of the magnetic non-potentiality. Combining the information provided by the helicity and the major flare, we deduce that the SSM finally becomes the major contributor of magnetic non-potentiality in the solar atmosphere in this AR. So for AR 10488, both twist of a single flux system and interaction of different flux systems contribute to the transport and accumulation of the non-potentiality, and the latter may be more effective than the former.

3.4. INDUCTION ELECTRIC FIELD

For better understanding of the buildup of the magnetic non-potentiality, we study the induction electric field, $\mathbf{E} = \mathbf{V} \times \mathbf{B}$, where $\mathbf{V}$ is the plasma velocity and $\mathbf{B}$ is the magnetic flux. $\mathbf{E}$ physically corresponds to the sweeping motion of magnetic field lines in the solar surface. The vertical velocity of the magnetic field lines can not be obtained directly. So here we discuss just the vertical component of $\mathbf{E}$. The magnetic field is approximately frozen in the plasma in the photosphere, and the normal velocity has no contribution to E_z. So we can take the transverse velocity computed by the LCT method instead of the horizontal velocity of the plasma. E_z shows the relationship between the horizontal motion and the transverse magnetic field.

Figure 7 shows gray scale maps of E_z. In the rotation phase, the maxima of E_z are located near the rotating or twisting areas of the main positive spot. In the shear phase, the maxima of E_z shift to the 'strong shear area' which is between the new positive and the old negative spots showing SSM. The maxima of E_z amount to $0.1 \sim 0.2\,\mathrm{V\,cm^{-1}}$, which are comparable with the electric field in the slow magnetic reconnection stage of the evolution of a two-ribbon flare ($0.1\,\mathrm{V\,cm^{-1}}$) reported by Wang *et al*. (2003).

The positions of the maxima of E_z imply that the parameter E_z possibly relates to magnetic non-potentiality in the solar atmosphere in this AR. In order to see more clearly the relationship between E_z and the non-potentiality, we have investigated a flare in this AR. On October 30, an M1.6 flare was observed by the HSOS Hα telescope. It began at 01:56 UT, reached its maximum at 02:07 UT, and ended at 02:29 UT. Figure 8 shows the Hα filtergram of this flare at 02:03 UT, superposed with the contours of $E_z = \pm 0.12\,\mathrm{V\,cm^{-1}}$ (the thick lines). From the Figure we find that there is no obvious correlation between the maxima of E_z and the bright kernels. However, in the 'strong shear area', E_z is intense, and the Hα filtergram presents a less bright strip (see the mark 'f' in Figure 8). This phenomenon remains

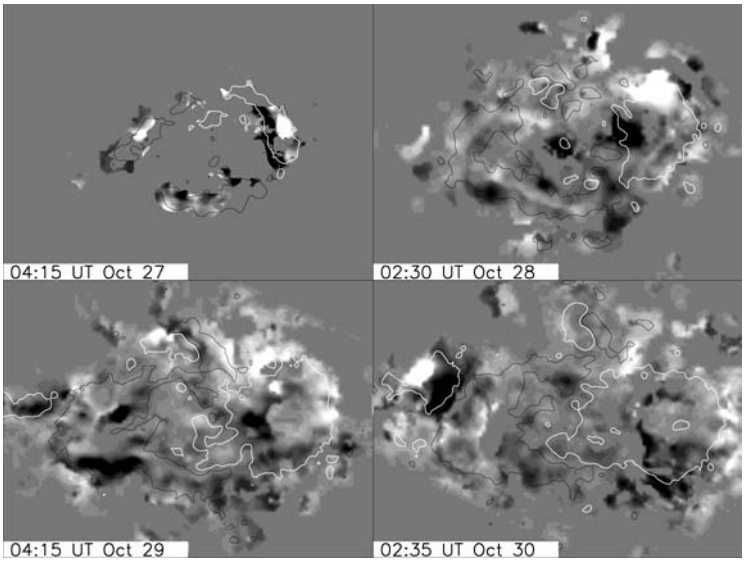

Figure 7. Gray scale maps of E_z. The *white* and *black contours* represent longitudinal magnetic field strengths of 200 and −200 G, respectively. The field of view is $225'' \times 168''$.

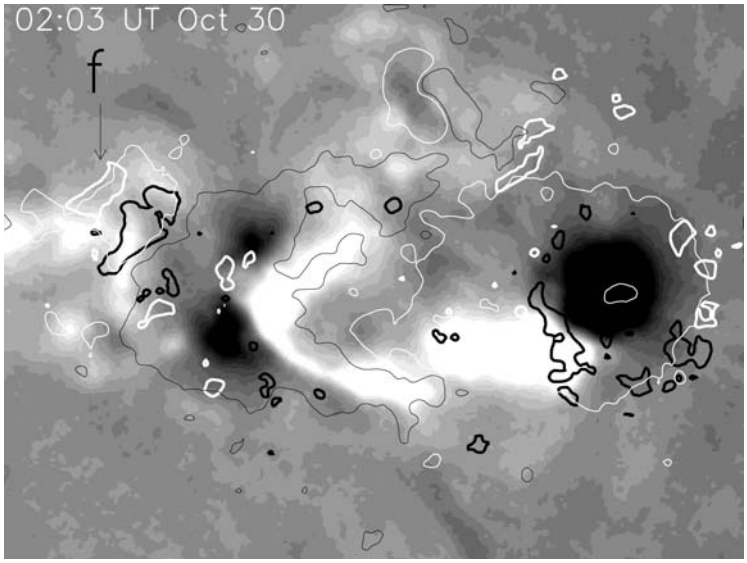

Figure 8. An M1.6 Hα flare observed at HSOS on October 30, the *thick white* and *black contours* represent the $E_z = \pm 0.12\,\mathrm{V\,cm^{-1}}$, and the *thin ones* longitudinal magnetic field strengths of ±200 G, the field of view is $225'' \times 168''$.

for a few hours around the flare time and deserves further investigation. Recalling the X-class flare kernels being located right between the new positive and the old negative spots at 01:25 UT on November 3, we suggest that the magnetic free energy is accumulated persistently by the SSM in this 'strong shear area'. We need full and accurate data of more flares, especially the powerful flares, to investigate the relationship between E_z and flare.

3.5. MAGNETIC HELICITY BUDGET

The average of $\mathrm{d}H/\mathrm{d}t$ is about $-5 \times 10^{41}\,\mathrm{Mx}^2\,\mathrm{h}^{-1}$ after the maturity of the main bipolar spots. Till 22:00 UT on October 31, the accumulated change of helicity has reached $-4 \times 10^{43}\,\mathrm{Mx}^2$, and the magnetic flux has reached about $\pm 3 \times 10^{22}$ Mx. If the accumulated change of helicity keeps increasing in absolute value at the speed of that after the maturity of the main bipolar spots, it will amount to $-6 \times 10^{43}\,\mathrm{Mx}^2$ at 00:00 UT on November 3. This represents high level of helicity in an AR. Chae, Moon, and Park (2004) produced lower helicity of $8 \times 10^{42}\,\mathrm{Mx}^2$ for another AR. The main reason for this difference seems to be in the difference in the magnetic fluxes of the studied ARs. Nindos and Andrews (2004) indicated that the amount of the stored pre-flare coronal helicity was small for flares without CMEs than for flares with CMEs, and that the maximal absolute coronal helicity for flares with CMEs is about $7 \times 10^{43}\,\mathrm{Mx}^2$ and the average is about $2.68 \pm 1.81 \times 10^{43}\,\mathrm{Mx}^2$. So the coronal helicity inferred from horizontal motion in AR 10488 is sufficient for one or two flares with CMEs before 00:00 UT on November 3. In fact, 17 C-class, 6 M-class and 2 X-class flares occurred in this AR during its disk passage. Identifying the time of flares and CMEs and scanning the movies of them obtained by the Large Angle and Spectrometric Coronagraph Experiment, we have found that there were 2 CMEs (occurred at 01:59 and 10:06 UT on November 3 separately) associated with the flares (X2.7 and X3.9 flares occurred at 01:09 and 09:43 UT on November 3 separately). It should be pointed out that the helicity of a single CME or MC depends on the length of the MC flux tube adopted (using the MC helicity computation as proxy to the CME helicity). If a shorter length of 0.5 AU is adopted, the mean helicity of a single CME or MC is typically $2 \times 10^{42}\,\mathrm{Mx}^2$ (DeVore, 2000). The coronal helicity inferred from horizontal motions in AR 10488 is much bigger than that. It is also comparable with the ones carried away by MCs (in the order of $10^{43}\,\mathrm{Mx}^2$) reported by Nindos, Zhang, and Zhang (2003), although no MC was linked to events originating from this AR.

4. Discussion

Differential rotation may be important for some ARs but it is negligible for most of the ARs in the generation process of magnetic helicity. (Chae, 2001, Chae *et al.*,

2002, Démoulin *et al*., 2002, Nindos, Zhang, and Zhang, 2003). Following Chae (2001), we make an estimation of the rate of helicity change by differential rotation for the region of our study based on equation (15) of DeVore (2000): $\mathrm{d}H/\mathrm{d}t = \pi/32\,\Omega \mathrm{F}^2$ with $\Omega = -8.6 \times 10^{-7} \sin b \cos^2 b\,\mathrm{s}^{-1}$. Using $F = 3.0 \times 10^{22}$ Mx and $b = 9^\circ$ for our observing area results in $\mathrm{d}H/\mathrm{d}t = -4.1 \times 10^{40}\,\mathrm{Mx}^2\,\mathrm{h}^{-1}$. This is a factor of 8 smaller than the average $\mathrm{d}H/\mathrm{d}t$ owing to the other horizontal motions.

Following Chae *et al*. (2001), we find that the arbitrary motions introduced by errors in v are very localized and do not affect our results more than $\pm 10\%$. The maxima of the absolute values of the derived velocities are about $0.8\,\mathrm{km\,s}^{-1}$ and the rms values of the derived velocity vectors are about $0.2\,\mathrm{km\,s}^{-1}$. There exist transverse velocities which are undetectable by LCT, e.g., motions along the isocontours of vertical component of the magnetic field (Démoulin and Berger, 2003). So we may underestimate the twist motions in the AR. The MDI measurements suffer from saturation in fields above 1.5–2 KG. This will make us underestimate the G in part of the positive main spot in regions of strong vertical magnetic field, thus underestimate the ΔH there. Nindos and Zhang (2002) found that when they multiply the MDI fields by a factor of 1.6 for $|B| > 500$ G, the resulting values of $\mathrm{d}H/\mathrm{d}t$ become 1.1–1.4 times higher than before. Using the uncorrected data of MDI, the helicity and flux we have computed are therefore lower limits.

The magnetic helicity includes both the twist and writhe helicities of a single flux system and the linkage of different flux systems, which are usually difficult to separate using photospheric observing data, especially in δ ARs. The twist and writhe are discussed very often in helicity and δ group formation studies, while the linkage is overlooked sometimes. Thus some information of the helicity is lost. The SSM in AR 10488, which has significant contribution to the build-up of helicity, probably relates to the linkage of different magnetic flux systems.

Some previous works reported the shearing motion (SM) seen near the polarity inversion line (PIL) inside a single flux system (Chae *et al*., 2001; Chae, Moon, and Park, 2004; Nindos and Zhang, 2002). It is worthwhile to compare our results with their works. Chae, Moon and Park (2004) studied the emerging process of AR NOAA 10365 from its birth. They reported that both the magnetic flux and helicity of the AR increased steadily and 4.5 days later reached 1.2×10^{22} Mx and $8 \times 10^{42}\,\mathrm{Mx}^2$, respectively. From their plots of flux and helicity as functions of time, we deduced that the ratio of H/F^2 keeps increasing for the first 4 days, reaches its peak value (about 0.09), then decreases for the following day to 0.05. This is quite consistent with the conditions in the rotation phase of our AR. A similar case has been found for AR NOAA 9165 studied by Nindos and Zhang (2002). They reported that the flux and helicity reaches 8×10^{21} Mx and $-6 \times 10^{42}\,\mathrm{Mx}^2$, respectively. We have deduced that the absolute value of their H/F^2 keeps increasing in the first 50 h during the emergence of the AR, reaches about -0.07, then becomes steady for about 10 h. Although the absolute value of H/F^2 continues to increase and reaches -0.1 after another 40 h, this latter increase occurs during the decay of the AR and has nothing to do with flux emergence. So we consider that the SM near the PIL

inside a single flux system has similar behavior in helicity transport to that of the twist, and the SM and twist may have similar origins below the photosphere which probably relate to the twist or writhe inside a single flux system. Considering the fact that the helicity transported by the SSM is 3 times larger than that of the twist in similar time duration for our AR, we suggest that the SSM between two different flux systems may have the ability to transport more magnetic helicity to the upper atmosphere than the SM near the PIL inside a single flux system, and that the SSM may have quite different origin below the photosphere which may relate to the linkage of different flux systems. These suggestions deserve further investigation.

The formation of the δ configuration in this AR belongs to the third formation type indicated by Zirin and Liggett (1987): collision of two distinct bipolar groups. A pair of new bipolar spots were born piggy-back style on the existing main spots and then the two adjacent opposite polarities shoved into and sheared strongly with each another. Thus a δ spot formed. Zirin and Liggett also indicated that such δ spots are not so active. The helicity accumulation of AR 10488 is somewhat higher than those of reported by Chae *et al*. (2001), Chae, Moon, and Park (2004) and Nindos and Zhang (2002). After the formation of the δ configuration, the helicity of the AR increases rapidly and steadily (see Figure 4). There is filament formation in the AR studied by Chae *et al*. (2001), magnetic clouds associated with the AR studied by Nindos and Zhang (2002), and 2 X-class flares in the AR studied by Chae, Moon, and Park (2004) during its emergence. However, before November 3, in a period of 7.5 days, no X-class flare or other intensive solar activity occurred in this AR. Indeed, AR 10488 is not so active in a relatively long time period of its emergence.

5. Summary

In this paper we have studied the evolution of the magnetic field, the magnetic helicity inferred from horizontal motions, the vertical component of current helicity, and the vertical component of induction electric field in the photosphere in a fast emerging flux region NOAA 10488. The twist of photospheric footpoints represents the rotation phase of the AR, and the strong shear motion (SSM) between two different flux systems represents the subsequent shear phase. The SSM brings more magnetic helicity into the corona than the twisting motion. After the maturity of the main bipolar spots, their twist decreases and the SSM becomes dominant and finally becomes the main contributor of magnetic non-potentiality in the solar atmosphere in this AR. So we consider that in this AR the interaction, which may relate to the linkage of different flux systems, brings more helicity into the upper atmosphere and appears to contribute more to the transport and accumulation of the non-potentiality than the twist of the single flux system. The coronal helicity inferred from the horizontal motions in this AR amounts to -6×10^{43} Mx^2. This is comparable with

the coronal helicity of ARs producing flares with CMEs or the helicity content of MCs reported in previous studies (Nindos, Zhang, and Zhang, 2003; Nindos and Andrews, 2004). The vertical component of the induction electric field, E_z, has been analyzed particularly. The maxima of E_z in our computation are about $0.1 \sim 0.2\,\mathrm{V\,cm^{-1}}$. We have found that the maxima of E_z are located in the twisting areas during the rotation phase, and shift to the 'strong shear areas' in the shear phase, which means that the parameter E_z possibly relates to the non-potentiality in the solar atmosphere in this AR. However, no obvious correlation is found between the kernels of Hα flare and E_z for the M1.6 flare in this AR, except for a less bright strip in the Hα filtergram in the 'strong shear area' which correlates with intense E_z, deserving further investigation. This paper also presents the formation and transport of helicity in a δ active region.

Acknowledgements

We are grateful to all members of SOHO/MDI consortium for providing the wonderful data. We thank Dr. Jongchul Chae for critical comments and suggestions that helped in improving the manuscript. We thank Dr. L. van Driel-Gesztelyi for helpful editorial work. One of the author, Jihong Liu, would like to give her thanks to Jiangtao Su, Yin Zhang, Mei Zhang, Shudong Bao, Xingming Bao and Jie Chen for their helpful discusses and advices. This work is supported by the National Natural Science Foundation of China under grants 10233050, 10233050, 10228307, 10311120115, 10473016 and by the National Basic Research Program of China under grant TG 2000078401.

References

Bao, S. D., Ai, G. X., and Zhang, H. Q.: 2001, *IAUS* **203**, 247.
Bao, S. D. and Zhang, H. Q.: 1998, *Astrophys. J.* **496**, L43.
Berger, M. A. and Field, G. B.: 1984, *J. Fluid Mech.* **147**, 133.
Berger, T. E. and Lites, B. W.: 2003, *Solar Phys.* **213**, 213.
Chae, J.: 2001, *Astrophys. J.* **560**, L95.
Chae, J., Moon, Y. J., and Park, Y. D.: 2004, *Solar Phys.* **223**, 39.
Chae, J., Wang, H. M., Qiu, J., Goode, P. R., Strous, L., and Yun, H. S.: 2001, *Astrophys. J.* **560**, 476.
Chen, J. M., Wang, H. M., and Zirin, H.: 1994, *Solar Phys.* **154**, 261.
Démoulin, P. and Berger, M. A.: 2003, *Solar Phys.* **215**, 203.
Démoulin, P., Mandrini, C. H., van Driel-Gesztelyi, L., Thompson, B. J., Plunkett, S., Kővári, Z., Aulanier, G., and Young, A.: 2002, *Astron. Astrophys.* **382**, 650.
Deng, Y. Y., Wang, J. X., Yan, Y. H., and Zhang, J.: 2001, *Solar Phys.* **204**, 13.
DeVore, C. R.: 2000, *Astrophys. J.* **539**, 944.
Gary, G. A. and Hagyard, M. J.: 1990, *Solar Phys.* **126**, 21.
Hagyard, M. J., Smith, J. B., Jr., Teuber, D., and West, E. A.: 1984, *Solar Phys.* **91**, 115.

Kim, J. S., Zhang, H. Q., Kim, J. S., Kim, K. S., and Bao, X. M.: 2002, *Chin. J. Astron. Astrophys.* **2**, 81.
Kusano, K., Maeshiro, T., Yokoyama, T., and Sakurai, T.: 2002, *Astrophys. J.* **577**, 501.
Leka, K. D., Canfield, R. C., McClymont, A. N., and van Driel-Gesztelyi, L.: 1996, *Astrophys. J.* **462**, 547.
Liu, Y. and Zhang, H. Q.: 2001, *Astron. Astrophys.* **372**, 1019.
Liu, Y. and Zhang, H. Q.: 2002, *Astron. Astrophys.* **386**, 646.
Moon, Y. J., Chae, J., Choe, G. S., Wang, H. M., Park, Y. D., Yun, H. S., Yurchyshyn, V., and Goode, P. R.: 2002a, *Astrophys. J.* **574**, 1066.
Moon, Y. J., Chae, J., Wang, H. M., Choe, G. S., and Park, Y. D.: 2002b, *Astrophys. J.* **580**, 528.
Nindos, A. and Andrews, M. D.: 2004, *Astrophys. J.* **616**, L175.
Nindos, A. and Zhang, H. Q.: 2002, *Astrophys. J.* **573**, L133.
Nindos, A., Zhang, J., and Zhang, H. Q.: 2003, *Astrophys. J.* **594**, 1033.
November, L. J. and Simon, G. W.: 1988, *Astrophys. J.* **333**, 427.
Seehafer, N.: 1990, *Solar Phys.* **125**, 219.
Tanaka, K.: 1991, *Solar Phys.* **136**, 133.
Tang, F.: 1983, *Solar Phys.* **89**, 43.
Wang, H. M., Qiu, J., Jing, J., and Zhang, H. Q.: 2003, *Astrophys. J.* **593**, 564.
Wang, J. X., Zhou, G. P., and Zhang, J.: 2004, *Astrophys. J.* **615**, 1021.
Wang, T. J. and Abramenko, V. I.: 2000, *Astron. Astrophys.* **357**, 1056.
Wang, T. J., Xu, A. A., and Zhang, H. Q.: 1994, *Solar Phys.* **155**, 99.
Yang, G., Xu, Y., Cao, W. D., Wang, H. M., Denker, C., and Rimmele, T. R.: 2004, *Astrophys. J.* **617**, L151.
Zhang, H. Q.: 2001a, *Astrophys. J.* **557**, L71.
Zhang, H. Q.: 2001b, *Mon. Not. R. Astron. Soc.* **326**, 57.
Zhang, H. Q., Bao, X. M., Zhang, Y., Liu, J. H., Bao, S. D., Deng, Y. Y., *et al.*: 2003, *Chin. J. Astron. Astrophys.* **3**, 491.
Zirin, H. and Liggett, M. A.: 1987, *Solar Phys.* **113**, 267.